POLITECNICO
MILANO 1863

School of Industrial and Information Engineering
Master of Science in Space Engineering

Course of Spacecraft Attitude Dynamics and Control
Professor Franco Bernelli Zazzera

Attitude Determination and Control of a 6U Earth Observation CubeSat

Group n° 26
Project n° 217

Person code	Last name	First name	Bachelor Degree and University
10691436	Casiero	Alessia	Aerospace Eng., Politecnico di Milano
10719352	Fiume	Elisa	Aerospace Eng., Politecnico di Milano
10766758	Gallo	Emanuele	Aerospace Eng., Politecnico di Milano
11015991	Marotta	Arianna	Aerospace Eng., Università degli Studi di Napoli Federico II

Academic Year 2023-2024

Contents

Introduction

The aim of this report is to investigate the attitude dynamics and control of a 6U CubeSat satellite on a LEO orbit. The analysis presents an ADCS design and a numerical simulation, which has been carried out by means of Matlab and Simlunk (version 2023b), for a remote sensing CubeSat mission. The focus of this project is on the first orbit, after the satellite is released by the launcher. In this condition, the spacecraft needs to perform different manoeuvres to properly orient and to maintain its pointing axis in the correct direction. The manoeuvres evaluated are: de-tumbling, slew and tracking. The maximum pointing error margins are set by the mission.
The first chapter includes the specifics on the mission, on the orbit, on all the hardware and configuration choices.
In the second chapter there is the implementation of dynamics and kinematics of the spacecraft, of the full model of environmental conditions that affect the satellite during its mission, the attitude determination and the design of the control system.
The last chapter presents the results showing the effectiveness of the control system.

	Assigned specification	**Modifications** (if any)	**Validation for modifications**
Platform	CubeSat	-	-
Attitude parameters	Quaternions	-	-
Mandatory sensors	Magnetometer	Sun Sensor Gyroscope	section 1.3
Actuators	3 reactions wheels	-	-

1. Mission specification

1.1 Spacecraft's model

The 6U CubeSat satellite chosen is the AYRIS-1 [1] [2]. It is equipped with solar panels, used as an energy source and made of silicon, hinged to the four sides of the spacecraft's structure. The specifics on the spacecraft's structure are listed in the table below, where, the satellite's surfaces have been divided into two categories: the ones belonging to the main core and the four solar panels.

Table 1.1: CubeSat properties

Component	**Material**	**Length** $[mm]$	**Width** $[mm]$	**Height** $[mm]$	**Weight** $[kg]$
Main body	Aluminium	100	200	300	8.9
Solar panel 1	Silicon	200	300	0.0035	0.49
Solar panel 2	Silicon	100	300	0.0035	0.24

In order to simplify the spacecraft's model, it has been assumed to be a rigid body with inertia axes coincident with the symmetry axes. The computation of the inertia properties of this satellite under evaluation has been done with the aid of the spacecraft model made on SolidWorks.

The data are evaluated with all four solar panels deployed and, for simplicity, they are considered constant during the whole simulation. The computed inertia matrix is:

$$I = \begin{bmatrix} 0.13 & 0 & 0 \\ 0 & 0.16 & 0 \\ 0 & 0 & 0.18 \end{bmatrix} [kgm^2] \qquad (1.1)$$

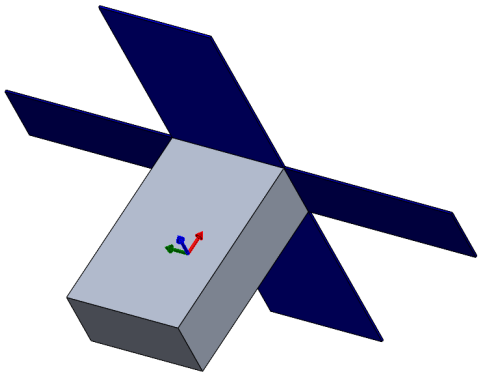

Figure 1.1: Spacecraft's model

The centre of mass is:

$$CoM = [0.02;\ 0.00;\ 0.00] \qquad (1.2)$$

1.2 Orbit's properties

It was hypothesised that the spacecraft would be used for Earth observation, which relies on nadir pointing with the requirement of a maximum pointing error of 1° with respect to nadir direction. During the mission, the satellite's imaging payload is pointed directly towards the Earth's nadir which is the point beneath the satellite. Its mission takes place in a LEO sun-synchronous orbit which is characterized by the Keplerian coordinates listed in the table below:

Table 1.2. Keplerian coordinates

a $[km]$	**e** $[-]$	**i** $[deg]$	**Ω** $[deg]$	**ω** $[deg]$	**θ** $[deg]$
6890.66	0.00149	97.525	104.0100	287.373	72.588

In order to propagate the full orbit, a simple 2-body problem with no perturbation has been considered:

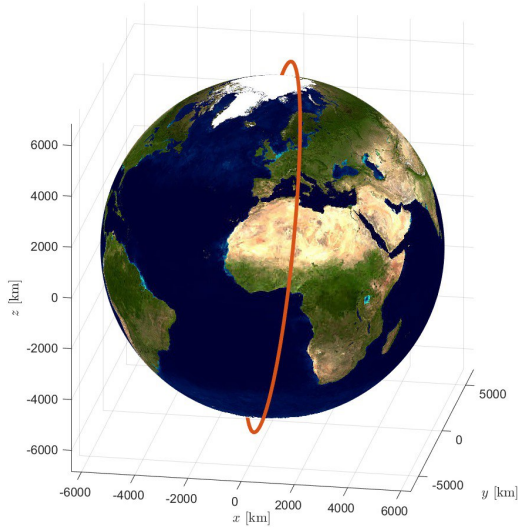

Fig. 1.2. Spacecraft's orbit

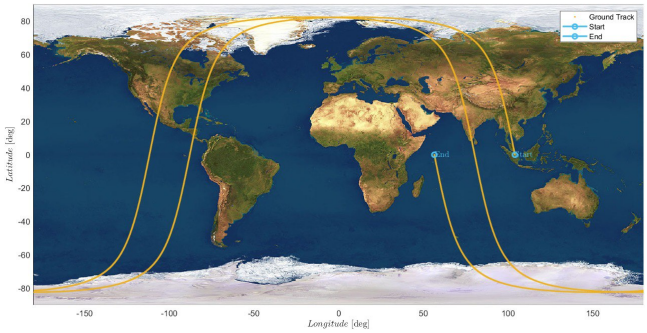

Fig. 1.3. Ground-track of the spacecraft for 2 orbits

1.3 Sensors

To achieve the determination of the spacecraft's attitude, a combination of sensors is employed. This includes a magnetometer, strategically positioned on an extendable boom, along with six Sun Sensors (one for each face of the satellite), and a gyroscope situated as close as possible to the spacecraft's centre of gravity.

For effective attitude determination, measurements from at least two vectors are required. However, the magnetometer is considered the least accurate attitude reference sensor. This is due to its susceptibility to noisy interference from on-board electronics and variations caused by solar wind and solar storms. To mitigate these challenges, the magnetometer is complemented by other sensors, namely a Sun sensor and a gyroscope.

The Sun sensor is preferred over a horizon sensor due to its higher precision, and it has been demonstrated that the satellite, located in a sun-synchronous orbit, never enters an eclipse. Nevertheless, since there could be instances when the Sun is not within the field of view (FOV) of the Sun sensor, a gyroscope is implemented. This provides crucial measurements of angular velocity, contributing to both the attitude determination process and the preliminary phase of control facilitated by the state observer.

Table 1.3. Number and position of sensors

Sensor type	**Number**	**Position**
Magnetic sensor	1	on a boom
Sun sensor	6	+ X-axis - X-axis + Y-axis - Y-axis + Z-axis - Z-axis
Gyroscope	1	close to CG

1.3.1 Magnetometer

A three-axis magnetic sensor, Honeywell HMC1043 [3], designed for low-field magnetic sensing has been chosen. To reduce the magnetic interference, which would lead to incorrect measurements, the magnetic sensor is mounted upon an extendable boom which is lengthened along the y-axis and such that inertia moments I_x and I_z are increased when deployed. However, for simplicity, the boom extension has not been taken into account for the computation of inertia moments. The specifics of the magnetic sensor are reported in the table below:

Table 1.4. Magnetometer specifications

Dimensions [mm]	**Weight** [mg]	**Resolution** [$Gauss$]	**Field Range** [$Gauss$]	**Bandwidth** [Hz]	**Resolution** [$Gauss$]	**Accuracy** [°]
3 x 3 x 1.4	25.6	120 10^{-6}	[-6, +6]	5 10^{6}	120 10^{-6}	15

An angle of 0.01 deg for non-orthogonality with respect to principal axis of measurement and of 1 deg of non-orthogonality with respect to secondary axes of measurement have been considered. The errors affecting the measurements of the magnetometer are listed in Table 1.5:

Table 1.5. Magnetometer errors

Linearity error [%FS]	**Hysteresis error** [%FS]	**Repeatability error** [%FS]
0.1	0.06	0.1

The magnetometer measurements have been modelled as:

$$\vec{b}_{meas} = A_e \, \vec{b}_B + \vec{n} \tag{1.3}$$

1.3.2 Sun sensor

Six sun sensors have been added to this model, positioned on each face of the CubeSat. The model NCSS-SA05 [4] has been chosen for its small dimensions and weight. In addition, its wide field of view is capable of an accurate determination of the Sun angle. Specifications are listed in the table below:

Table 1.6. Sun sensor specifications

Dimensions [mm]	**Weight** [g]	**FoV** [°]	**Accuracy** [°]
33 x 11 x 6	5	114	<0.5

Knowing the direction of the sun with respect to sun sensor axes, it is possible to estimate the angles between the direction of solar rays with respect to the Sun sensor's axes. After having verified that the sun is in the FOV of each sensor, it is possible to evaluate which sensor is most exposed to sun radiation by selecting the one with minimum angles, e.g. the sensor whose z axis is almost parallel to the direction of the sun. Considering possible errors in the measurements, due to sun sensor accuracy, the sun direction measured by sun sensor is evaluated.

1.3.3 Gyroscope

The high-performance 3-axis gyroscope STIM210 [5] has been chosen to directly evaluate the angular velocity of the spacecraft. Its specifications are listed in the table below:

Table 1.7. Gyroscope specifications

Dimensions [mm]	**Weight** [g]	**Full Scale** [rad/s]	**Resolution** [$^\circ/\sqrt{h}$]	**Sampling Frequency** [Hz]
44.8 x 38.6 x 21.5	52	±400	0.22	262

In the present work, ARW, RRW and misalignment errors have been taken into account.

Table 1.8. Gyroscope errors

Angular Random Walk $[^\circ/\sqrt{h}]$	**RRW** $[^\circ/h^{\frac{3}{2}}]$	**Misalignment error** $[rad]$
0.15	0.0003	$1 \ \ 10^{-3}$

The noisy measurements of the gyroscope can be modelled:

$$\begin{cases} \vec{\omega}_i^M = \vec{\omega}_i + \vec{n} + \vec{b} \\ \vec{n} = \sigma_n \ \vec{\zeta}_n \\ \dot{\vec{b}} = \sigma_b \ \vec{\zeta}_b \end{cases} \tag{1.4}$$

Where $\vec{n}$ is the Angular Random Walk (ARW) with zero-mean white Gaussian noise and standard deviation σ_n, while $\dot{\vec{b}}$ is the Rate Random Walk (RRW) with zero-mean white Gaussian noise and standard deviation σ_b. In particular, the value for the standard deviations are: $\sigma_n = 0.15 \ \frac{deg}{\sqrt{h}} \frac{1}{\sqrt{T_s}}$ and $\sigma_b = 0.0003 \ \frac{deg}{h^{\frac{3}{2}}} \frac{1}{\sqrt{T_s}}$. Physically speaking, the former is related to the thermo-mechanical noise of the system, characterized by the ARW, while the latter is associated with the electronic noise, expressed through the RRW.

1.4 Actuators: Reaction Wheels

The purpose of the actuator is to apply a control torque to the spacecraft. In the model being examined, three small-size and low-cost reaction wheels TA6494 Series [6], inertial actuators, have been inserted and aligned with the three principal axes. Their specifications are reported in the table below:

Table 1.9. Reaction wheels specifications

Dimensions $[mm]$	**Weight** $[g]$	$\boldsymbol{I_r}$ $[kg \ m^2]$	$\boldsymbol{\omega_{r,max}}$ $[rpm]$	$\boldsymbol{h_r}$@ $4000rpm$ $[N \ m \ s]$	$\boldsymbol{M_r}$@ $4000rpm$ $[N \ m]$
$\phi 98 \ x \ 65$	> 1100	$7.0 \ x \ 10^{-4}$	5000	0.3	0.02

Where the mounting error is interpreted as a 0.1 $[kg/m^2]$ offset on the diagonal terms of the inertia matrix. The values of h_r, ω_r and M_r are computed:

$$\begin{cases} \vec{h}_r = I_r \vec{\omega}_r \\ \dot{\vec{h}}_r = -A^{-1}(\vec{M}_r + \vec{\omega}_{gyro} \times A\vec{h}_r) \\ \vec{M}_r = -\vec{\omega}_{gyro} \times A\vec{h}_r - A\dot{\vec{h}}_r \end{cases} \tag{1.5}$$

Where $\vec{\omega}_{gyro}$ is the angular velocity evaluated by the gyroscope. Then, these values are confronted with the values reported in the Table 1.9 to evaluate the presence of eventual saturation. No other actuators have been inserted since, in the present simulation, reaction wheels never saturate.

2. Model description

2.1 Dynamics

In order to evaluate the attitude dynamics, which allows us to describe the motion of the spacecraft around the Earth, it is reasonable to assume the satellite as a rigid body. The dynamics in a reference frame attached to the body can be expressed through Newton's second law:

$$\vec{M} = \dot{\vec{h}} + \vec{\omega} \times \vec{h} \tag{2.1}$$

Considering that the direction of the body frame axes coincides with that of the principal axes of inertia of the spacecraft and that the origin of the reference frame is centred in the centre of mass, dynamics can be simplified into a set of first-order differential equations known as Euler's equations:

$$\begin{cases} I_x\dot{\omega_x} + (I_z - I_y)\omega_y\omega_z = M_x \\ I_y\dot{\omega_y} + (I_x - I_z)\omega_x\omega_z = M_y \\ I_z\dot{\omega_z} + (I_y - I_x)\omega_x\omega_y = M_z \end{cases} \tag{2.2}$$

2.2 Kinematics

From the knowledge of initial conditions and angular velocities, computed from Euler's equations taking as input the torques around the axes, it is possible to build the evolution of spacecraft around the orbit at every time instant. The set of attitude parameters assigned to represent the evolution of one frame with respect to another is quaternions, a normalized vector of four parameters that can be divided into a vectorial part and a scalar variable [1]:

$$\vec{q} = [(q_1\, q_2\, q_3)\, q_4]^T = [\boldsymbol{q_v}\, q_4]^T \tag{2.3}$$

From the computation of the derivative of the quaternions with the expressions below, it is possible to propagate attitude performing the integration and then normalizing the expression to eliminate numerical errors:

$$\frac{d\vec{q}}{dt} = \lim_{\Delta t \to 0} \frac{\vec{q}(t + \Delta t) - \vec{q}(t)}{\Delta t} = \frac{1}{2}\Omega\vec{q}(t) \tag{2.4}$$

[1] In this work the first three elements of $\vec{q}$ are chosen to form the vectorial part and the fourth component is the scalar variable

$$\frac{d}{dt}\begin{bmatrix} q_1 \\ q_2 \\ q_3 \\ q_4 \end{bmatrix} = \frac{1}{2}\begin{bmatrix} 0 & \omega_z & -\omega_y & \omega_x \\ -\omega_z & 0 & \omega_x & \omega_y \\ \omega_y & -\omega_x & 0 & \omega_z \\ -\omega_x & -\omega_y & -\omega_z & 0 \end{bmatrix}\begin{bmatrix} q_1 \\ q_2 \\ q_3 \\ q_4 \end{bmatrix} \tag{2.5}$$

Although the lack of physical interpretation of quaternions, the main advantage of the use of this set of parameters is to be searched in the absence of geometrical singularities and the low computational expense of the kinematic differential equations.

2.3 Environmental modelling

2.3.1 Orbit propagation

The orbit is propagated at every time step of the simulation. First, the true anomaly is evaluated through the integration of the following equation:

$$\dot{\theta} = \frac{n(1+ecos\theta)^2}{(1-e^2)^{\frac{3}{2}}} \tag{2.6}$$

With $n = \sqrt{\frac{GM_T}{a^3}}$ for an almost circular orbit. Then, the position vector is computed as:

$$r_N = \frac{a(1-e^2)}{1+ecos\theta} \tag{2.7}$$

Also, the Sun direction is evaluated in the inertial frame through the relation:

$$\hat{S}_N = r_{Sun}\begin{bmatrix} cos(n_{Sun}t) \\ sin(n_{Sun}t)cos\epsilon \\ sin(n_{Sun}t)sin\epsilon \end{bmatrix} \tag{2.8}$$

Where: $n_{Sun} = \frac{2\pi}{T}$ with $T = 1$ year, r_{Sun} is the distance Earth-Sun and $\epsilon = 23.45°$.
In addition, the quaternion representing the LVLH frame (orbit frame) is computed as:

$$q_{LN} = q(\Omega) \otimes (q(i) \otimes q(\omega+\theta)) = \begin{bmatrix} 0 \\ 0 \\ sin(\frac{\Omega}{2}) \\ cos(\frac{\Omega}{2}) \end{bmatrix} \otimes \left(\begin{bmatrix} sin(\frac{i}{2}) \\ 0 \\ 0 \\ cos(\frac{i}{2}) \end{bmatrix} \otimes \begin{bmatrix} 0 \\ 0 \\ sin(\frac{\omega+\theta}{2}) \\ cos(\frac{\omega+\theta}{2}) \end{bmatrix} \right) \tag{2.9}$$

2.3.2 Disturbing torques

The disturbing torques considered in the model under evaluation are the gravity gradient torque, the Earth's magnetic field torque, the solar radiation pressure torque and the torque due to atmosphere drag. The total disturbing torque is computed as:

$$\vec{M}_d = \vec{M}_{GG} + \vec{M}_{magnetic} + \vec{M}_{SRP} + \vec{M}_{aerodynamic} \tag{2.10}$$

After the implementation of all the torques, only the two most relevant disturbances have been considered in the present simulation: magnetic and gravity gradient torques, as can be seen in Figure 2.1 and in Table 2.1, in which a first analytical estimation of the maximum values of the four torques has been computed and compared with the values obtained from the simulation.

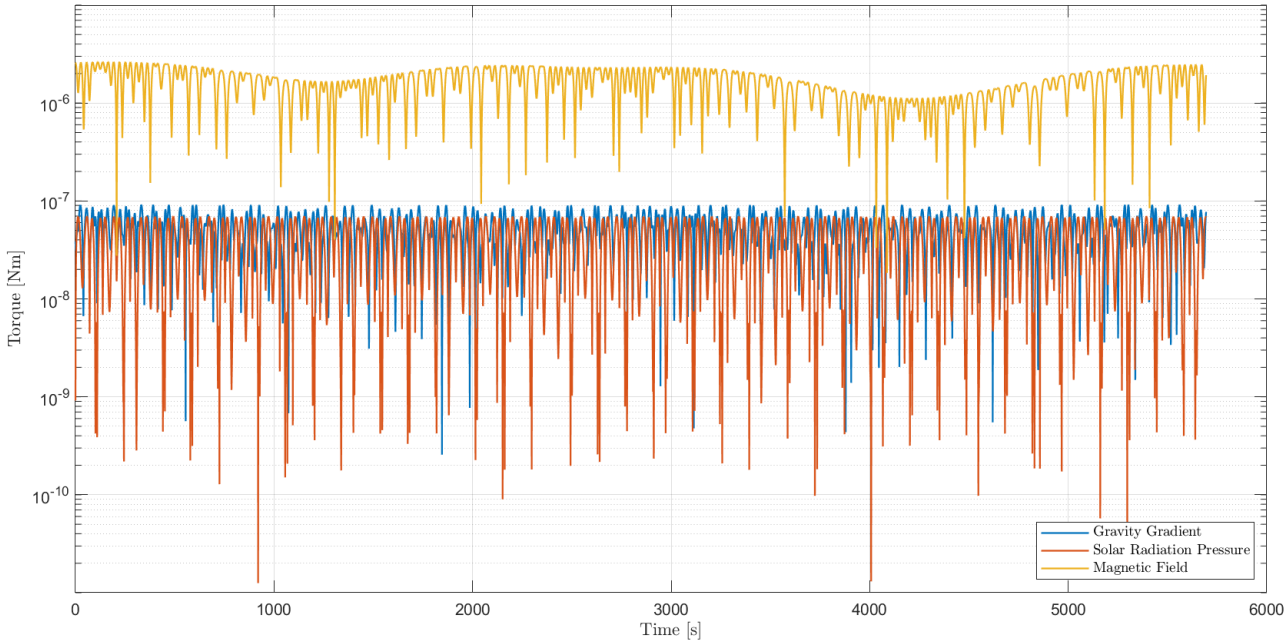

Fig. 2.1. Norm of environmental disturbances

Table 2.1. Maximum Torques

Torque $[Nm]$	Analytical max value	Simulation max value
Gravity gradient	$1.1514\ 10^{-7}$	$1.1296\ 10^{-7}$
Magnetic	$2.5423\ 10^{-6}$	$3.6160\ 10^{-6}$
SRP	$5.4846\ 10^{-8}$	$9.6787\ 10^{-8}$
Aerodynamic	$1.0145\ 10^{-10}$	–

2.3.2.1 Gravity gradient torque

Due to the not uniformity of the gravity field, a torque acts on the satellite. This effect is particularly relevant for large satellites and for a long time of action. In the principal inertia

reference frame, this torque can be modelled as:

$$\vec{M}_{GG} = \frac{3Gm_t}{R^3} \begin{bmatrix} (I_z - I_y)c_2c_3 \\ (I_x - I_z)c_1c_3 \\ (I_y - I_x)c_1c_2 \end{bmatrix} \tag{2.11}$$

Where:

- R = orbital radius, distance between the centre of Earth and the centre of the satellite
- $c_1,\ c_2,\ c_3$ are the direction cosines of the radial direction in the principal axes

It can be noted that if one of the principal axes is aligned with the radial direction, the disturbances due to gravity gradient vanish.

2.3.2.2 Magnetic torque

The magnetic torque which acts on the satellite depends on its position and attitude and it is generated by the interaction between $\vec{m}$, the residual magnetic induction due to electrical currents in the satellite, which constitutes an undesired effect, and $\vec{B}$, the external magnetic field:

$$\vec{M}_{magnetic} = \vec{m} \times \vec{B} \tag{2.12}$$

Where, as the value of the residual dipole moment, it was chosen: $\vec{m} = [0.01\ 0.05\ 0.01]^T\ Am^2$ to represent a conservative scenario for estimating torque. The Earth's magnetic field is more intense at the poles and decreases with the inverse of the cubic power of the distance to the ground, halving at the equator and can be expressed as the gradient of potential:

$$\begin{cases} B_r = -\frac{\partial V}{\partial r} \\ B_\theta = -\frac{1}{r}\frac{\partial V}{\partial \theta} \\ B_\phi = -\frac{1}{r\ sin\theta}\frac{\partial V}{\partial \phi} \end{cases} \tag{2.13}$$

The simplest approach to model the Earth's magnetic field is by approximating it with a dipole field. However, such an approximation is valid only for altitudes above 7000km. For the selected low orbit altitude in this study, a more complex model has been employed. The potential function is expressed as a series of spherical harmonics, where each term is weighted by Schmidt quasi-normalized Legendre polynomials.

$$V(r,\theta,\phi) = R\sum_{n=1}^{k}\left(\frac{R}{r}\right)^{n+1}\sum_{n=1}^{k}(g_n^m cos(m\phi) + h_n^m sin(m\phi))P_n^m(\theta) \tag{2.14}$$

Where r is the distance from the centre of Earth, θ is the colatitude, ϕ is the longitude, R is the Earth's equatorial radius, g_n^m and h_n^m are Gaussian parameters retrieved from experimental data available from tables of IGRF (International Geomagnetic Reference Field) and $P_n^m(\theta)$ = Schmidt quasi-normalized Legendre functions of degree n and order m.

The data used for the model were taken from IGRF 2000 and a 13^{th}-order-expansion of the above equation was applied (k = 13) [7].

The components of the magnetic field $\vec{B}$ expressed in the geocentric inertial reference frame are:

$$\begin{cases} B_x = (B_r cos\delta + B_\theta cos\delta) cos\alpha - B_\phi sin\alpha \\ B_y = (B_r cos\delta + B_\theta sin\delta) sin\alpha + B_\phi cos\alpha \\ B_z = (B_r sin\delta - B_\theta cos\delta) \end{cases} \tag{2.15}$$

Where δ is the satellite declination and α is the right ascension, evaluated as: $\alpha = \phi + \alpha_G$. Through the rotation $\vec{B}_B = q'_{BN} \otimes [\vec{B}_N; 0] \otimes q_{BN}$, the magnetic field is then measured in the body frame.

The two figures below report the contour plots of the magnitude of the magnetic field for the value of altitude $h = 500\ km$ from the ground and for a 13^{th}-order-expansion of the magnetic field model. The image on the right has been created using a software developed by the Finnish Meteorological Institute.

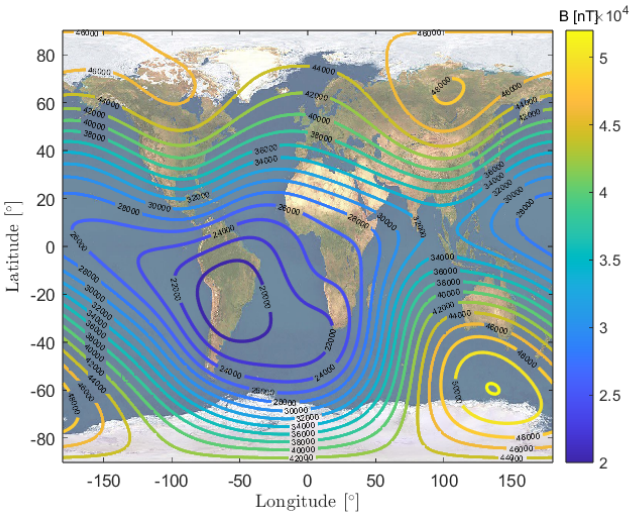

Fig. 2.2. Simulated IGRF2000 13^{th} order at 500 km (nT)

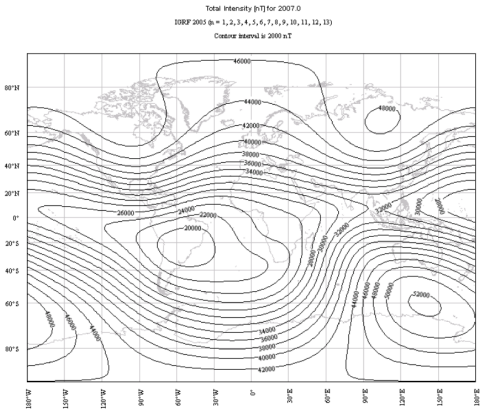

Fig. 2.3. IGRF 2005 13^{th} order at 500 km (nT)

2.3.2.3 Solar Radiation Pressure

The pressure induced on the sunlit surfaces of the satellite due to solar radiation results in a force and consequently a torque. This torque is inversely proportional to the square of the distance to the ground and can be considered nearly constant for geocentric orbits, given that the distance from the Sun is significantly greater than the orbital altitude. The electromagnetic radiation impacting the satellite comprises not only direct solar radiation but also torques generated by Earth-reflected radiation and Earth radiation itself. However, the latter two are notably influenced by the distance to the ground. The radiation values at an altitude of 500 km are provided in the table below:

Table 2.2. Radiation Contributions

Solar Radiation [W/m^2]	**Reflected Radiation** [W/m^2]	**Earth Radiation** [W/m^2]
1358	600	150

To model such disturbance torque, it must be taken into account the fact that not the whole incident radiation is absorbed, but a part is reflected with a specular or diffuse reflection. The model of the force acting on each exposed face of the satellite is reported below:

$$\vec{F_i} = -PA_i \ (\hat{S}_B \cdot \hat{N}_{B_i}) \Big[(1-\rho_s) \ \hat{S}_B + (2\rho_s \ (\hat{S}_B \cdot \hat{N}_{B_i}) + \frac{2}{3}\rho_d \Big] \ \hat{N}_{Bi} \tag{2.16}$$

Where:

- $P = \frac{F_e}{c}$ with c speed of light and F_e the solar radiation intensity
- $\hat{S}_B$ = direction pointing from the Sun to the satellite in the body frame
- $\hat{N}_{B_i}$ = normal direction to the i-surface of satellite in the body frame
- ρ_s and ρ_d = coefficient of specular reflection and of diffuse reflection, respectively

The coefficient of absorption can be retrieved by the following relation: $\rho_a + \rho_d + \rho_s = 1$.

Table 2.3. Coefficient of specular and diffuse reflection of spacecraft and solar panels

	Spacecraft	**Solar panels**
ρ_s	0.5	0.1
ρ_d	0.1	0.1

The overall torque is given by the sum of all the contributions given by each surface of the spacecraft which are not in a shadowed region:

$$\vec{M}_{SRP} = \begin{cases} \sum_{i=1}^{n} \vec{r_i} \times \vec{F_i} & \hat{S}_B \cdot \hat{N}_{B_i} > 0 \\ 0 & \hat{S}_B \cdot \hat{N}_{B_i} < 0 \end{cases} \tag{2.17}$$

Given the position vector of the spacecraft and the position vector of the Sun, it has been proven that the satellite in the orbit under evaluation never goes into eclipse [9]. Assuming that the shadow created by the Earth is a cylindrical projection of the Earth's diameter along the direction of the Sun to Earth, which is a good approximation for low-altitude orbits, the spacecraft goes into eclipse if:

$$\vec{r} \cdot \frac{\vec{S_N}}{|\vec{S_N}|} < -\sqrt{(r^2 - R_e^2)} \tag{2.18}$$

Where: $\vec{r}$ is the spacecraft position vector, $\hat{S}_N$ is the unit vector in the Earth-Sun direction and R_e is the equatorial radius of the Earth, which is approximated as a sphere.

2.3.2.4 Aerodynamic torque

Since the estimated value of the aerodynamic torque is not relevant compared to the others, it is considered negligible in the model under evaluation.

2.4 Control and determination algorithms

2.4.1 Attitude Determination algorithm

The measurements provided by sensors must be converted in order to obtain complete knowledge of the attitude of the spacecraft. Since the kinematics has been modelled using quaternions, the solution adopted, despite its computational cost, is the q-method, which belongs to the category of statistical methods. For such methods, the knowledge of the measures of two or more directions in space and the relative precision of the sensors are required to build and minimize the weighted error function. In this approach, the exact solution is the one which minimizes the weighted error function, which is the aim of Whaba's problem. However, since an exact solution to the problem cannot be reached due to the presence of measurement errors, the optimal solution, which could minimize the cumulative sum of errors, is to be reached:

$$J = \frac{1}{2} \sum_{i=1}^{N} \alpha_i |s_i - A\ v_i|^2 \tag{2.19}$$

Where: α_i are the weights associated to each measurement representing the accuracy of the sensor and are generally normalized to sum one, s_i and vi are the unit vectors measured by sensors in body-fixed and inertial frame, respectively, and A is the Direction Cosine Matrix (DCM), rotation matrix between the body and inertial frame.

With the adoption of the q-method, the cost function changes and the solution of Whaba's problem becomes simpler. The expression of the attitude matrix is replaced by its representation in terms of quaternions:

$$A = (q_4^2 - \underline{q}^T \underline{q})I + 2\underline{q}\underline{q}^T - 2q_4[\underline{q} \times] \tag{2.20}$$

The cost function to minimize becomes:

$$J = \sum_{i=1}^{N} \alpha_i - \underline{q}^T K \underline{q} \tag{2.21}$$

Where K is a 4x4 matrix:

$$K = \begin{bmatrix} S - \sigma I & z \\ z^T & \sigma \end{bmatrix} \tag{2.22}$$

With:

- $B = \sum_{i=1}^{N} \alpha_i s_i v_i^T = [b_{ij}]$
- $S = B^T + B$
- $z = [b_{23} - b_{32};\ b_{31} - b_{13};\ b_{12} - b_{21}]$
- $\sigma = tr(B)$

This corresponds to maximize function:

$$\tilde{J} = \underline{q}^T K \underline{q} \tag{2.23}$$

Adding the constraint $qq^T = 1$ embedded with Lagrange multiplier λ, the function to maximize becomes:

$$\tilde{G} = \underline{q}^T K \underline{q} - \lambda(qq^T - 1) \tag{2.24}$$

Evaluating the gradient of $\tilde{G}$ and imposing it to zero, the obtained eigenvalue problem is: $K\underline{q} = \lambda \underline{q}$. Then, substituting it into the expression of $\tilde{J}$, it is obtained: $\tilde{J}(q) = \lambda$. The optimal attitude is the eigenvector associated with the maximum eigenvalue λ of matrix K.

2.4.2 Attitude control

After the spacecraft is launched and reaches its position for the actual scientific mission to take place, the attitude control system is responsible for the achievement of the desired attitude. As previously mentioned, the objective of the control system is to achieve Nadir pointing with a mean pointing error below 1° in a reasonable time. After a preliminary filtering by the state observer, three main phases, performed by exploiting the assigned actuators, can be distinguished: detumbling phase, slew manoeuvre, tracking phase.

2.4.2.1 State observer

The state observer is a fictitious system which allows to compute an estimation of the state of the real system x by processing its output y. This initial stage in control implementation becomes necessary due to the inevitable presence of noise in sensor measurements, which can affect their reliability. The concrete benefit of this computational and modelling effort is a relevant cost-saving as it eliminates the need for additional sensors or actuators to enhance control. The implemented logic involves a linear state observer, operating on a linear model of the system. This leads to linear relationships between the inputs, states, and outputs of the observer. The observer's dynamics in the discrete-time case follows the subsequent mathematical model:

$$\hat{x}(k+1) = \hat{A}\ \hat{x}(k) + L\ (y(k) - \hat{y}(k)) \tag{2.25}$$

Where L is the gain of the observer. The quantities we want to observe are angular velocity and attitude, expressed through quaternion. The dynamics of the angular velocity under the discrete-time hypothesis is:

$$I\vec{\omega}(k+1) = \vec{M}_D(k) + \vec{M}_C(k) + I\vec{\omega}(k) \times \vec{\omega}(k) \tag{2.26}$$

Looking at the state space model: $\hat{A}_\omega = I^{-1}\frac{\vec{M}_D(k)+\vec{M}_C(k)+I\vec{\omega}(k)\times\vec{\omega}(k)}{\vec{\omega}(k)}$.
Therefore, the related observer is:

$$\vec{\omega}_{est}(k+1) = \hat{A}_\omega\vec{\omega}_{obs}(k) + L_\omega(\vec{\omega}_{gyro}(k) - \vec{\omega}_{est}(k)) \tag{2.27}$$

Where $\vec{\omega}_{gyro}(k)$ is the variable to be observed in a precise way and L_ω is determined by statistical analysis.
The dynamics of the attitude quaternion under the discrete-time hypothesis is:

$$q_{est}(k+1) = \frac{1}{2}\Omega q_{est}(k) \tag{2.28}$$

So that: $\hat{A}_q = \frac{1}{2}\Omega$. The related observer is:

$$q_{est}(k+1) = \hat{A}_q q_{est}(k) + L_q(q(k) - q_{est}(k)) \tag{2.29}$$

2.4.2.2 Detumbling phase

After the spacecraft is released from the launcher, the tumbling motion of the satellite is inevitable. For that reason, the first phase to take place is the de-tumbling. The primary objective of this phase is to reduce the spacecraft's angular velocity until it aligns with the desired value of $\vec{\omega_d} = [0, 0, 0]$, thereby achieving a stable configuration. To achieve such a purpose, a proportional control has been applied:

$$\vec{M}_{detumbling} = -k_d\ (\vec{\omega} - \vec{\omega}_d) \tag{2.30}$$

With tuning parameter $k_d = 0.03$, selected using the trial-and-error method.

2.4.2.3 Slew manoeuvre

After the detumbling phase is completed and the angular velocity matches the desired value, a slew manoeuvre corresponding to an eigenaxis rotation is performed to reach the correct pointing conditions to retrieve the spacecraft's attitude, orienting it towards the desired target $q_D = q_{LVLH}$ (Paragraph 2.3.1, Equation 2.9) while maintaining the desired value of $\vec{\omega_d}$ unchanged with respect to the previous phase. The slew controller selected, chosen such that $\dot{V} < 0$ according to Lyapunov's second stability theorem, is:

$$\vec{M}_{slew\ manoeuvre} = \vec{\omega}\times I\vec{\omega} - k_1 I\vec{\omega} + k_2 I\frac{\partial H(q_{4e})}{\partial q_{4e}}\vec{q_e} \tag{2.31}$$

Where k_1 and k_2 are tuning parameters set to 0.4 and 0.06, respectively and $q_e = q'_{LN}\otimes q_{BN}$ and $H(q_{4e})$ is the potential function, which is a function of the scalar part of the quaternion. It is important to select the best-performing potential function. In the present model it has been chosen as:

$$H(q_{4e}) = 1 - {q_{4e}}^2 \tag{2.32}$$

The potential function chosen satisfies the conditions of the Lyapunov function for which: $H(\pm 1) = 0$ and $H(q_{4e}) > 0$ for $q_{4e} \neq \pm 1$, so that the zero error state $\vec{\omega} = 0$ is a stable equilibrium point, solving the problem of unwinding.

2.4.2.4 Trajectory tracking - Earth pointing

After the slew manoeuvre is completed, a tracking phase is needed to maintain the attitude conditions reached by the spacecraft in previous phase. This phase consists in following a time-varying attitude q_{LVLH} while maintaining the desired angular velocity $\vec{\omega}_d = [0, 0, n]$. Such a maintenance phase lasts until the end of the orbital period.

$$\vec{M}_{tracking} = -k_1\vec{\omega}_e + k_2\frac{\partial H(q_{4e})}{\partial q_{4e}}\vec{q}_e + \vec{\omega} \times I\vec{\omega} + I\frac{d}{dt}(A_e(q)\vec{\omega}_d) \tag{2.33}$$

Where $k_1 = 0.5$ and $k_2 = 0.07$ and $\vec{\omega}_e = \vec{\omega}_B - A_e(q)\vec{\omega}_d$.

2.5 ADCS architecture

Figure 2.4 displays the conceptual diagram block in which the full model used in the present work is represented.

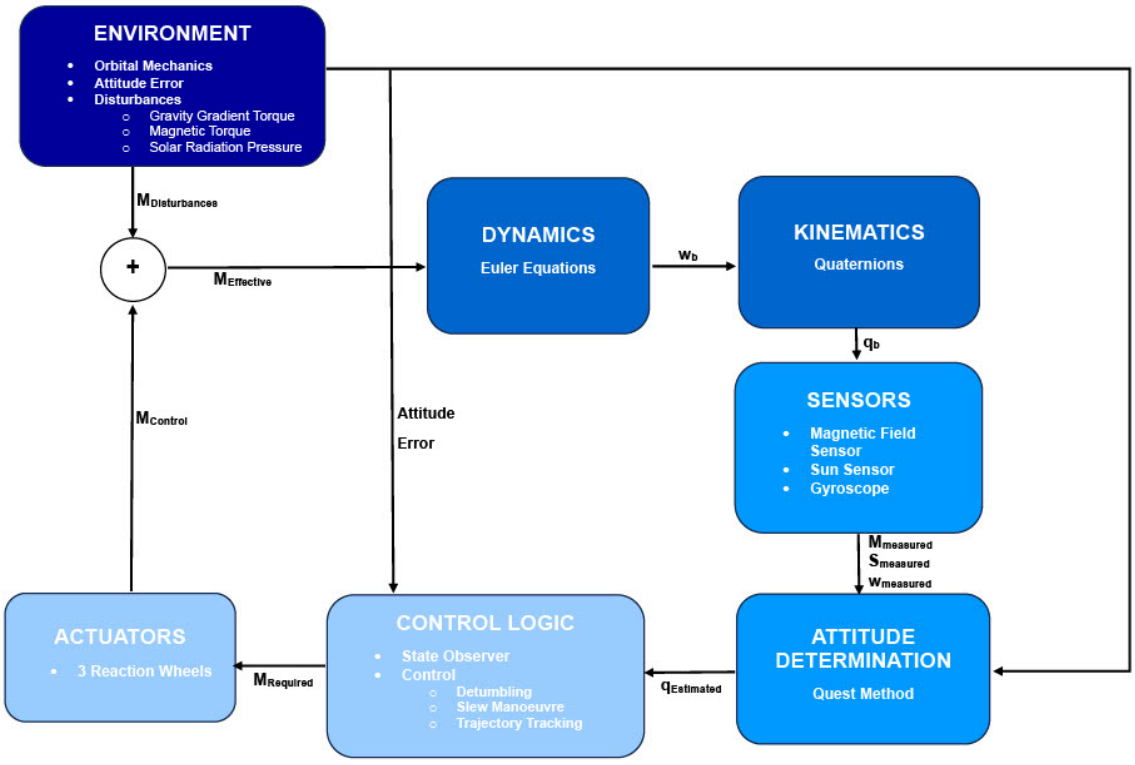

Fig. 2.4. Model's block diagram

3. Results

3.1 Fixed initial conditions

As initial conditions in terms of dynamics and attitude of the rigid body the following have been taken: $\vec{\omega}_0 = [-5, 3, 2]$ $[deg/s]$ and $\vec{q}_0 = [0, 0, 0, 1]$. The maximum detumbling time is set to 1000 s, while it is 4000 s for the slew manoeuvre from the beginning of the control (at 0 s). The simulation stop time is set to two orbits. Figure 3.1 shows the pointing error for all the phases of the mission, highlighting that, when the tracking phase starts, the average value of pointing error is less than 0.5°, completely fulfilling the requirement of pointing accuracy. Pointing error is computed as 2 $tan(||\vec{q}_e||/q_{4e})$.

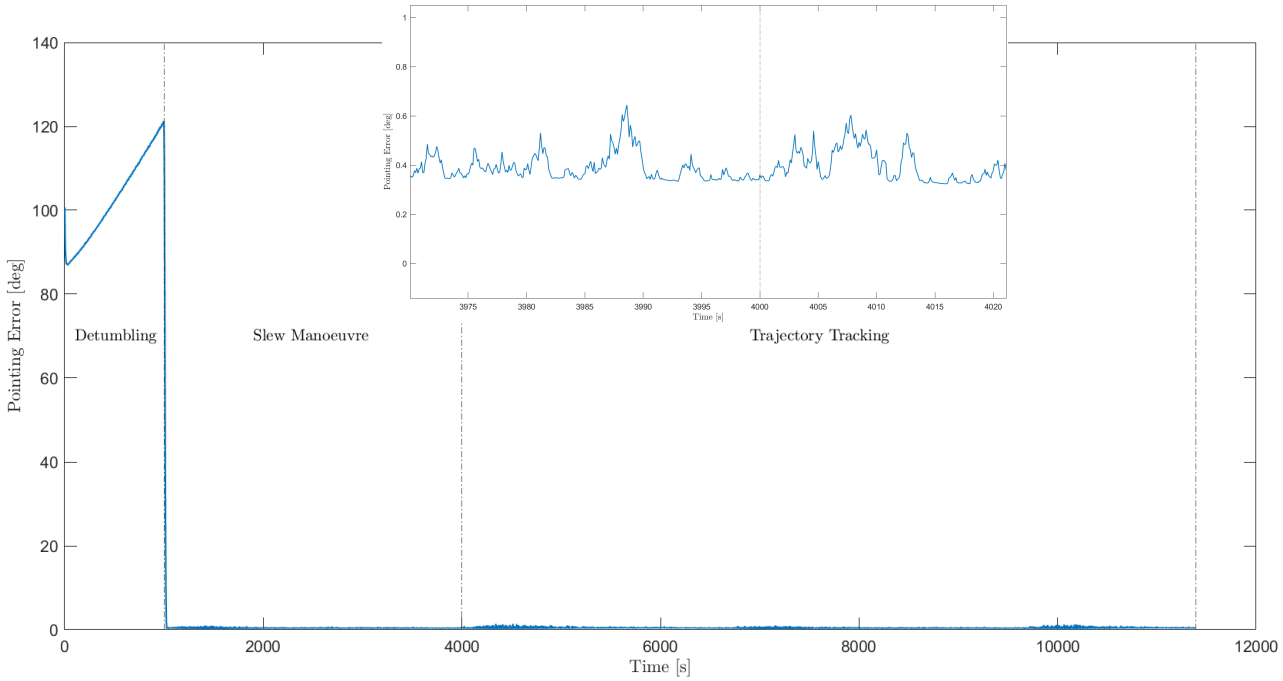

Fig. 3.1. Pointing error

In Figure 3.2 it is reported the angular velocity filtered by the state observer, while in Figure 3.3 it is plotted the angular velocity error $\vec{\omega}_e$, whose components go to zero. Furthermore, to verify that the desired attitude is reached, in Figure 3.4 the convergence to zero of the quaternion error $\vec{q}_e$ is shown. In the end, Figure 3.5 displays the control torque given by the reaction wheels during the whole mission.

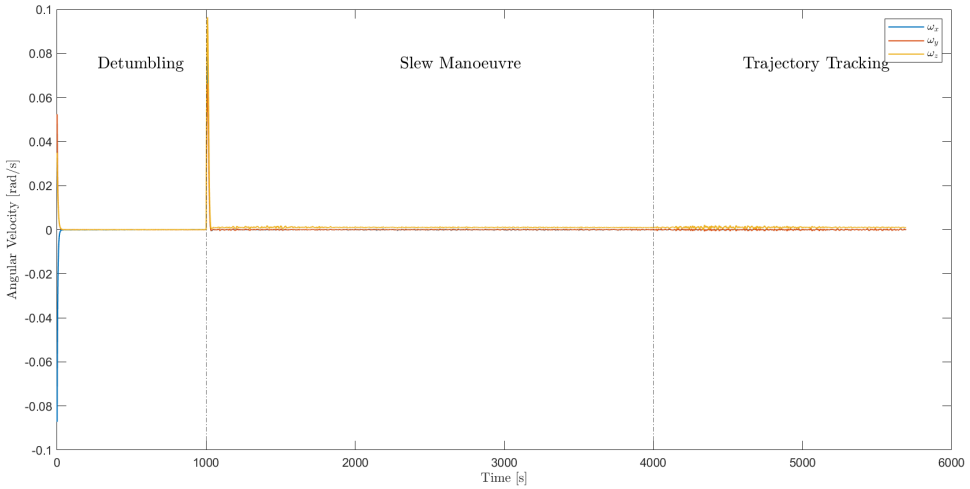

Fig. 3.2. Angular velocity

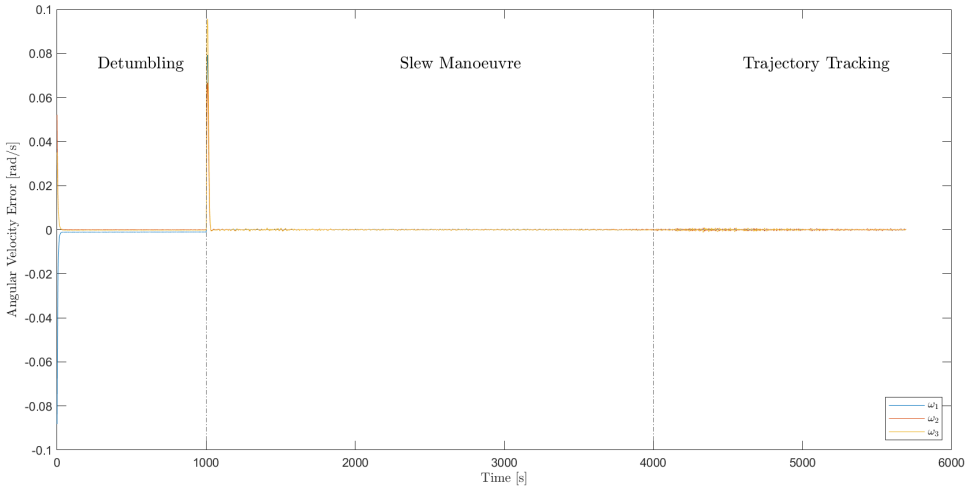

Fig. 3.3. Angular velocity error

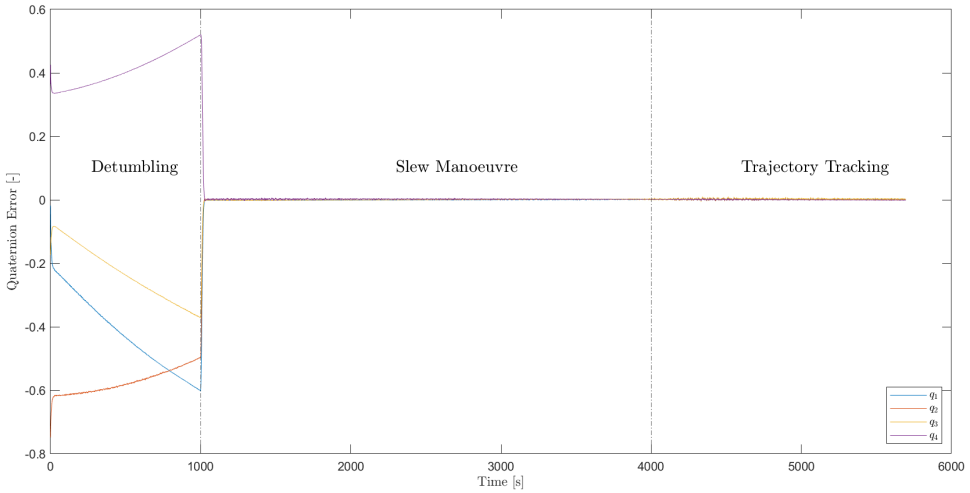

Fig. 3.4. Quaternion error

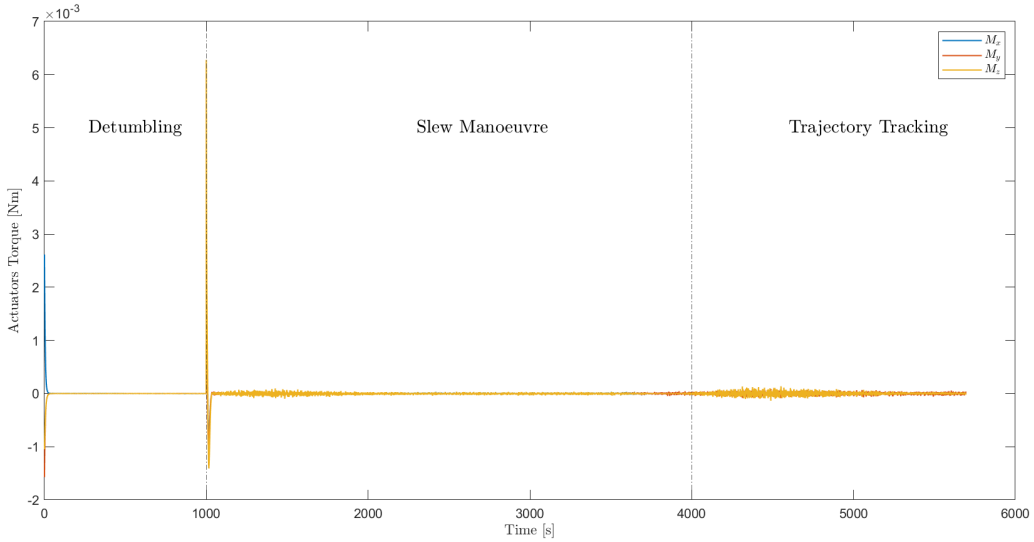

Fig. 3.5. Actuators Torque

3.2 Control free

To evaluate the effect of the environment on the satellite, demonstrate the effectiveness and the need to have attitude control, a test without the control action has been performed, selecting as initial conditions the ones for which the spacecraft configuration is perfectly oriented and spinning at the desired rate ($\vec{\omega}_d$ and $\vec{q}_d$). As shown in Figure 3.6, the pointing requirements are completely lost.

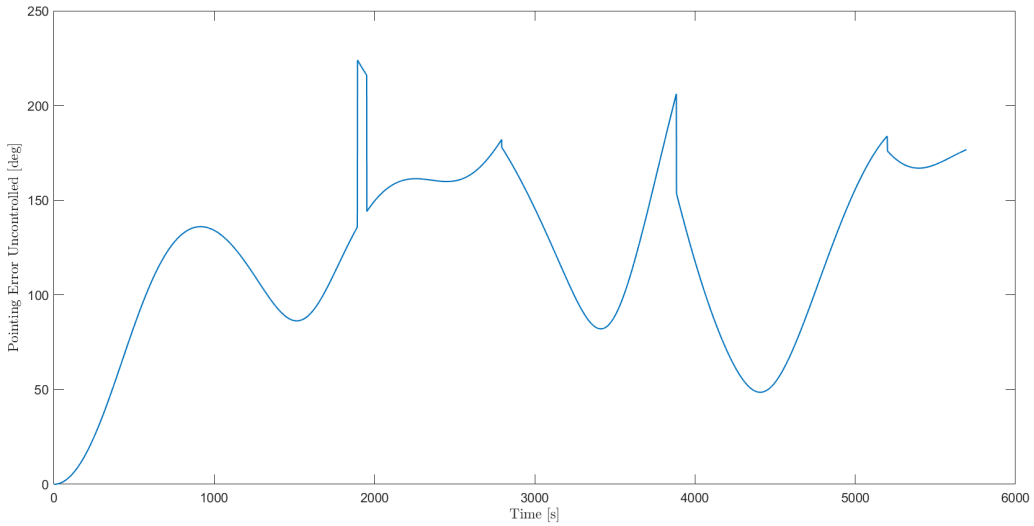

Fig. 3.6. Pointing error - control free case

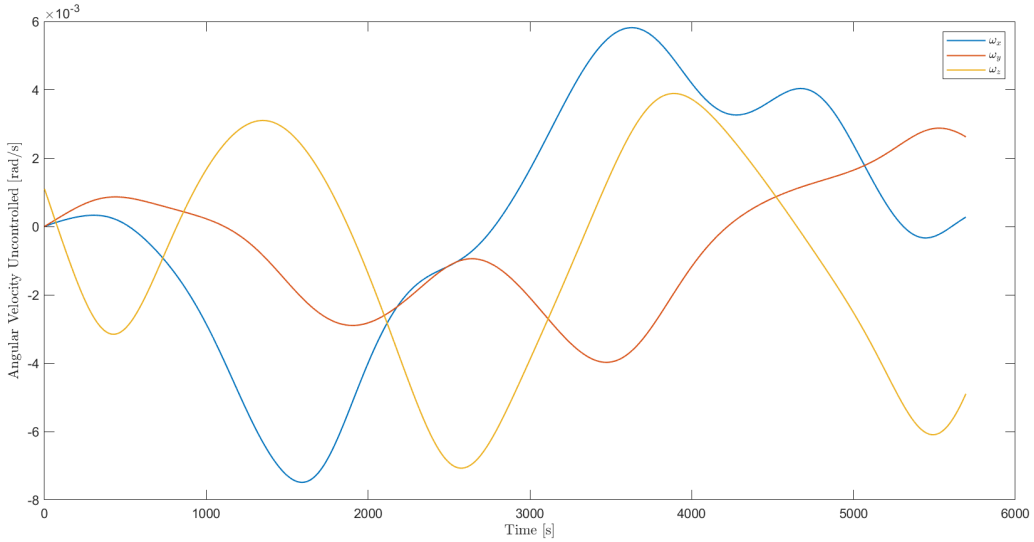

Fig. 3.7. Angular velocity - control free case

3.3 Random analysis

In order to test the robustness of the controller, a study with random initial conditions has been implemented as can be seen in Figure 3.8 and 3.9. The outcomes reveal the controller's effective performance across various simulated scenarios.

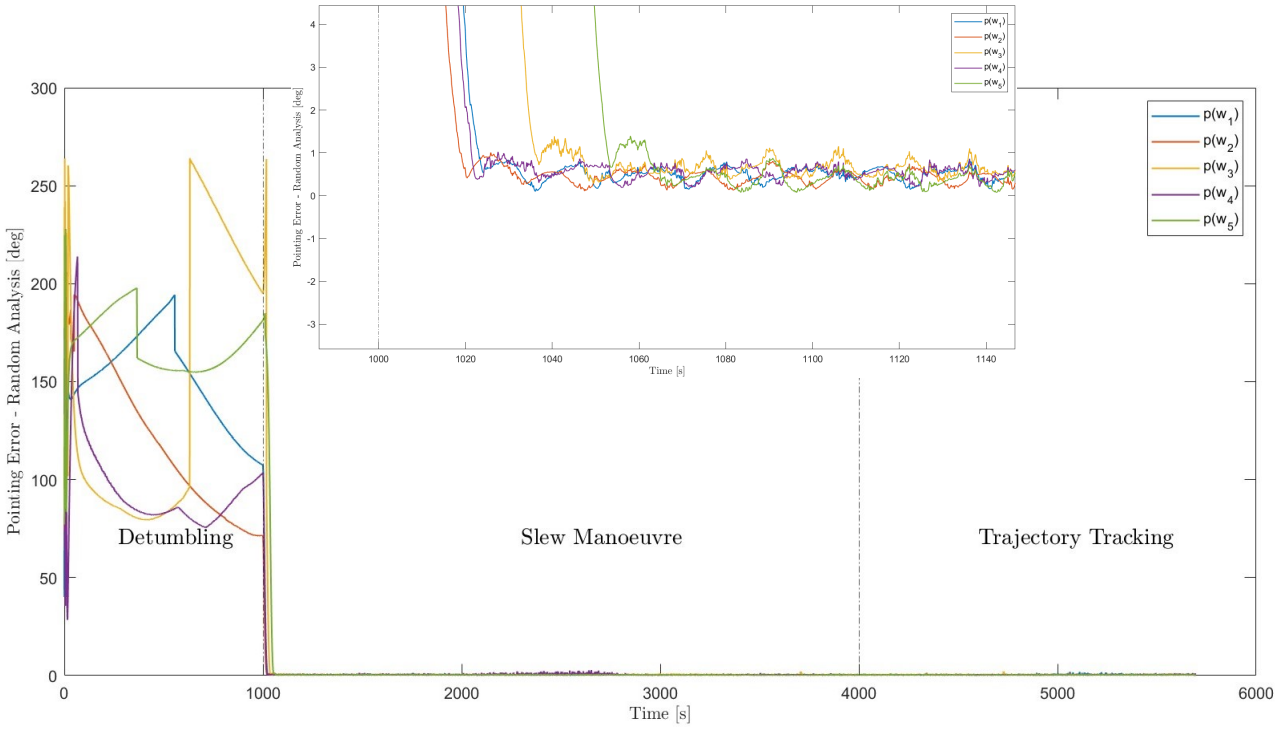

Fig. 3.8. Pointing error Random analysis

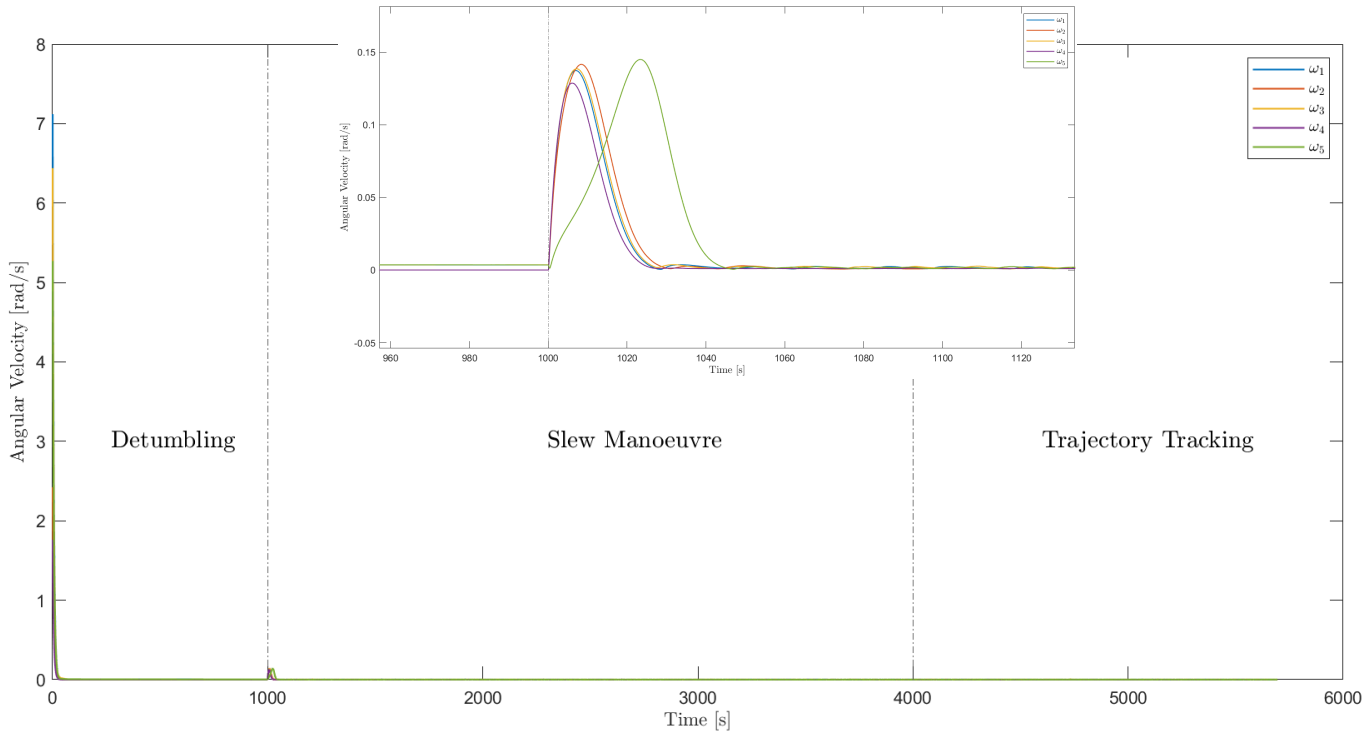

Fig. 3.9. Angular velocity Random analysis

3.4 Conclusions

By incorporating randomly generated initial values for angular velocity, the system demonstrates the ability to successfully execute detumbling, slew, and maintain nadir-pointing orientation within a timeframe of less than 2000 seconds. It is noteworthy that this duration is less than a single orbital period for the specific orbit under consideration, with a period denoted as $T = 5689.60$ seconds. Importantly, these achievements satisfy all the requirements imposed on the Attitude Determination and Control System (ADCS).

Upon close examination and comparison with an uncontrolled scenario, the indispensable role of the control system in reorienting and stabilizing the satellite becomes evident when subjected to perturbations. The controlled system outperforms the uncontrolled case, demonstrating the effectiveness of the implemented control strategy. The robustness of the control system is further validated through the comprehensive analysis of random scenarios. This additional evaluation highlights the system's ability to adapt and effectively manage varying conditions, substantiating its reliability in real-world operational scenarios.

Bibliography

[1] *Ayris Nanosats Database*
https://www.nanosats.eu/sat/ayris

[2] *In-the-sky.org*
https://in-the-sky.org/spacecraft.php?id=56988

[3] *3-Axis Magnetic Sensor HMC1043*
https://www.arrow.com/en/products/hmc1043/honeywell

[4] *Sun Sensor NCSS-SA05*
https://satsearch.co/products/newspace-systems-ncss-sa05-coarse-sun-sensor

[5] *STIM210 Multi-axis Gyro Module*
https://www.sensonor.com/products/gyro-modules/stim210

[6] *RW TA6494 Series - Reaction Wheel | SatCatalog*
https://www.satcatalog.com/component/rw-ta6494-series/

[7] International Geomagnetic Reference Field
https://www.ngdc.noaa.gov/IAGA/vmod/igrf.html

[8] Jeremy Davis, *Mathematical Modeling of Earth's Magnetic Field Technical Note*, 2004, Virginia Tech, Blacksburg, VA 24061

[9] F. Landis Markley and John L. Crassidis, *Fundamentals of Spacecraft Attitude Determination and Control*, Springer, New York, 2014

[10] Franco Bernelli Zazzera, *Spacecraft Attitude Dynamics – Course Notes*, Politecnico di Milano, 2023-2024